Wireless Torque Pulsations Measurement System for PMSMs

Maria Martinez, Daniel Fernandez, David Reigosa, Juan Manuel Guerrero and Fernando Briz
Dept. of Elect., Computer & System Engineering, University of Oviedo, Gijón, Spain
martinezgmaria@uniovi.es, fernandezalodaniel@uniovi.es, diazdavid@uniovi.es, guerrero@uniovi.es, fernando@isa.uniovi.es

***Abstract*— Torque pulsations are one of the major concerns in permanent magnet synchronous machines (PMSMs). Torque pulsations can be mitigated by proper machine design and/or by control. Independently of the means being used, precise measurement of torque pulsation is highly desirable for the validation and improvement of machine designs and control strategies. This paper proposes a non-invasive, wireless vibration measurement system aimed to provide precise estimates of torque pulsations. The system is mounted on the rotor shaft of the PMSM, i.e. there is no mechanical coupling, and allows on-line measurement without interfering with the normal operation of the machine.[1]**

Keywords—Permanent Magnet Synchronous Machines, Torque vibrations, Cogging Torque, Torque Ripple.

I. Introduction

Permanent magnet synchronous machines (PMSMs) provide high efficiency, high torque and power density and good dynamic response compared to other types of electrical machines [1]-[4]. These features have made PMSMs widely used in a large variety of high performance applications such as automotive, robotics, servo drive, military, aerospace, etc. [5]-[8].

One of the major concerns in PMSMs operation are torque pulsations (smooth torque production) [9]-[13]. Torque pulsations in PMSM result from: a) interaction between PMs and the stator slot opening, i.e. cogging torque; b) non-sinusoidal distribution of the stator windings, c) non-sinusoidal current waveform or d) non-sinusoidal back-EMF [9]-[13], i.e. electromagnetic torque ripple. Reduction of torque pulsations is always desirable but can be critical in some applications [6]. Torque pulsations can be mitigated by proper machine design, e.g. using dummy slots [15], [18], stator slots skewing [15], magnet shifting [14], the use of fractional number of slots per pole [14] or magnet magnetization patterns [16], but still they cannot be fully eliminated. In addition to machine design, strategies based on feedforward harmonic compensation using proper control strategies have been proposed for torque pulsation reduction [11], [17]. Implementation of these methods can be difficult and involve a significant commissioning effort, as they require precise measurement of the torque pulsations (i.e. magnitude and phase angle of each relevant harmonic component), which are a function of machine's operating condition (torque, speed, temperature, …).

Accurate torque ripple measurement can be useful for multiple purposes, including assessment and validation of new machine designs, assessment/optimization of control strategies aimed to reduced torque pulsations or fault detection (e.g. demagnetization) in existing machines. Existing torque pulsation measurement systems include: torque transducers based on strain gauges [19]-[23], [25]-[28], Ferraris sensor [19], piezoelectric accelerometers [19], MEMs accelerometers [29], acceleration estimation using rotary encoder [19] and a weight variation of a beam attached to the rotor [24]. Unfortunately, all these methods suffer from some limitations. Rotary torque transducers are the most common option [20]; however, these sensors are relatively bulky, and introduce flexible elements in the shaft, reducing the torsional resonant frequency and eventually the measuring frequency range of the whole system [25]. In addition, they are scaled to measure the average torque (dc component of the torque), what can seriously compromise their resolution measuring torque pulsations since only a small portion of the measuring range will be excited by the torque pulsation; furthermore, often they are also sensitive to radial forces applied in the direction perpendicular to their axis of measurement (i.e. centrifugal forces) producing cross coupling between axis and creating magnitude errors in the torque measurement [20]-[23], [26]. Wireless transmission of strain gauge signals direct attached to the rotor shaft by means of telemetry and wireless power supply (induction, batteries) was reported in [27]-[28]. This eliminates the need of additional couplings, what results in lighter and smaller sensors. However, these sensors were also scaled to measure the average torque and have a reduced bandwidth, what compromises their capability to measure the torque ripple at high rotational speed. A beam attached to the rotor was proposed in [24] to measure cogging torque; however, its use is limited to zero speed, which is an obvious limitation. Systems based on Ferraris sensors, rotary encoders and piezoelectric accelerometer [19] have been proposed to measure torque ripple from the shaft angular acceleration. Ferraris sensors and piezoelectric accelerometers [19] measures the angular acceleration directly from the rotor shaft, however the

[1]This work was supported in part by the Research, Technological Development and Innovation Programs of the Spanish Ministry Economy and Competitiveness of the Spanish Government under the project MINECO-17-ENE2016-80047-R, in part by the Government of the Principality of Asturias under grant Severo Ochoa PA-20-PF-BP19-010 and the project IDI/2018/000188, by the University of Oviedo under grant PAPI 2018-PF-12, in part by grants of the European Regional Development Fund (FEDER funds) and by Thyssenkrupp under grant CAT-003-17.

attachment to the shaft increases the overall system inertia and requires additional mechanical couplings. Rotary encoders obtain the angular acceleration as the second derivative of the measured rotor angle. A concern for this method is that for a given torque ripple, the ripple in the acceleration is proportional to the torque ripple, but the ripple in the speed decreases inversely proportional to speed, and the ripple in the position, which is the measured quantity, decreases inversely proportional to the rotor speed squared. This makes this method highly imprecise at medium-high speeds. Measuring the tangential acceleration using two MEMs accelerometers using a differential configuration was proposed in [29]. The use of two accelerometers allows to compensate the effect of gravity. But places additional concerns due to impact of assembly/mounting tolerances and delays in the sampling of both signals on the effectiveness of the differential action.

This paper presents a wireless, shaft-mounted torque pulsation measurement system [30]. The system is mainly intended for the assessment/optimization of machine designs and control strategies aimed to provide smooth torque, i.e. to reduce torque pulsations. Further potential uses would include degradation/fault detection.

Similar to the encoder based method, the proposed method also uses the relationship between torque and acceleration (1) [1], [19], [29], [32], where α_r is the angular acceleration and J is the overall system inertia.

$$T_{out} = J\alpha_r \tag{1}$$

However, in the proposed system, shaft acceleration is measured directly using an accelerometer, avoiding the double integration which occurs when the position is measured. The use of a single accelerometer also reduces possible sources of measurement errors, simplify the data transmission, reduce the number of required devices and allows to synchronize all measured data with the rotor position using the gravity. Strengths of the proposed system include: high bandwidth; high accuracy and independent of the average torque and speed; no mechanical couplings, and consequently no risk of additional resonances; no interference with the normal operation of the machine. It is finally noted that though the paper will focus on PMSMs, the system can be used with any type of rotating machines or elements in general suffering from torque pulsations.

The paper is organized as follows: the physics of torque pulsations in PMSMs and FEA results are discussed in section II; main characteristics of torque ripple measurement using strain gauges based torque sensors are analyzed in section III; the proposed shaft-mounted accelerometer-based torque pulsations measurement system is described in section IV; experimental results are shown in section V. Finally, conclusions are presented in section VI.

II. Torque in PMSMs

Physical principles of average torque and torque pulsations in PMSMs are analyzed in this section.

A. Analytical torque model

Output torque of a PMSM can be modeled as the rate of change of the magnetic field co-energy [2],[33]-[34], (2).

$$T_e = \frac{dW_c}{d\theta_m} = \frac{P}{2}\frac{dW_c}{d\theta_e} \tag{2}$$

where W_c stands for the magnetic co-energy, P is the number of poles, θ_m is the rotor mechanical angle and θ_e is the rotor electrical angle. The magnetic co-energy of a PMSM assumed to be operating in a linear zone of the magnetizing curve is given by (3) [2], [34],

$$W_c = \frac{1}{2} i_{abc}^T l_{abc} i_{abc} + i_{abc}^T \lambda_{abc} + W_{cPM} \tag{3}$$

where l_{abc} is the abc inductance matrix, $i_{abc}=[i_a\ i_b\ i_c]^T$ and $\lambda_{abc}=[\lambda_a\ \lambda_b\ \lambda_c]^T$ are the phase current and magnet matrixes, respectively.

It is seen from (3) that the magnetic co-energy of a PMSM consists of three terms: the first term on the right hand side is due to the armature current; the second term is due to the interaction between the armature current and the PM flux and finally, the third term is due to the PM flux. By substituting (3) into (2), (4) is obtained.

$$\begin{aligned} T_e &= \frac{P}{2}\left(\frac{1}{2} i_{abc}^T \frac{dl_{abc}}{d\theta_e} i_{abc} + i_{abc}^T \frac{d\lambda_{abc}}{d\theta_e}\right) + T_{cog} \\ &= T_{rel} + T_{syn} + T_{cog} \end{aligned} \tag{4}$$

In a PMSM, the first term in (4) is the reluctance torque T_{rel}, which appears when the windings inductance varies with rotor position. The second term in (4) is the mutual torque or synchronous torque (T_{syn}), which appears due to the mutual magnetic flux linking the magnet and the coil. Finally, the last term in (4) accounts for the cogging torque (T_{cog}), which is produced by the interaction among magnets and stator teeth, and tries to align the rotor PMs with the minimum reluctance path through the stator teeth [2], [33]. T_{cog} is mainly determined by the machine design. Its harmonic order for a rotor revolution is given by (5) [10],[15],[18], where Q is the number of slots of the machine and LCM stands for the least common multiple between the number of stator slots and poles. T_{cog} can be expressed by (6) [10], [18], where T_{Ncogn} and ϕ_{Ncogn} are the magnitude and phase angle of the nN_{cog} harmonic component of the torque.

$$N_{cog} = LCM(Q, P) \tag{5}$$

$$T_{cog} = \sum_{n=1}^{\inf} T_{N_{cog}n} \cdot \cos(nN_{cog}\omega_r t + \phi_{N_{cog}n}) \tag{6}$$

In the ideal case of a sinusoidal distribution of PM magnetic field, winding and stator currents, T_{syn} (4) would be constant (i.e. without any torque ripple). However, non-sinusoidal distributions which are intrinsic to real machine designs, as well as the non-ideal behavior of the inverter feeding the machine will induce torque pulsations.

For the particular case of three-phase machines, torque harmonic components occur at integer multiples of six times the fundamental electrical frequency, T_{syn} (7) [2], where T_0 is the average synchronous torque, T_{6n} and ϕ_{6n} are the magnitude

and phase angle of the n·6th harmonic component of the torque with n being an integer number and ω_e the electrical excitation frequency.

$$T_{syn} = T_0 + T_{ripple} = T_0 + \sum_{n=1}^{\inf} T_{6n} \cdot \cos(n6\omega_e t + \phi_{6n}) \quad (7)$$

To take into account the spatial harmonics of the inductance and flux, l_{abc} and λ_{abc} in (4) can be divided into DC and harmonic components as follows:

$$T_e = \frac{P}{2}\left(\frac{1}{2} i_{abc}^T \frac{dl_{abch}}{d\theta_e} i_{abc} + i_{abc}^T \frac{d\lambda_{abch}}{d\theta_e} + \frac{1}{2} i_{abc}^T \frac{dl_{abc0}}{d\theta_e} i_{abc} + i_{abc}^T \frac{d\lambda_{abc0}}{d\theta_e}\right) + T_{cog} \quad (8)$$

where the subscripts "$_h$" and "$_0$" stand for harmonic and fundamental values, respectively. Eq. (8) can be rewritten as (9) [33]-[34].

$$T_e = \frac{P}{2}\left(\frac{1}{2} i_{abc}^T \frac{dl_{abch}}{d\theta_e} i_{abc} + i_{abc}^T \frac{d\lambda_{abch}}{d\theta_e} + \lambda_{abc0}^T \times i_{abc}\right) + T_{cog} \quad (9)$$

where "×" stands for the cross-product. Transforming (9) to a reference frame synchronous with the rotor (10) is obtained [33], where λ_{dqs0}^r is the fundamental flux linkage vector and the first and second terms in the right side of (10) account for the derivative of the harmonic content of the dq-axes inductances and dq-axes fluxes respectively.

$$T_e = \frac{3P}{4}\left(\frac{1}{2} i_{dqs}^{rT} \frac{dl_{dq}}{d\theta_e} i_{dqs}^r + i_{dqs}^{rT} \frac{d\lambda_{dqs}^r}{d\theta_e} + \lambda_{dqs0}^{rT} \times i_{dqs}^r\right) + T_{cog} \quad (10)$$

Expressing λ_{dqs0}^r as (11) and substituting (11) into (10), the average and harmonic torque components of a PMSMs can be finally obtained as (12).

$$\lambda_{dqs0}^r = \begin{bmatrix} L_d i_{ds}^r + \Lambda_{PM} \\ L_q i_{qs}^r \end{bmatrix} \quad (11)$$

$$T_e = \frac{3P}{4}\left(\frac{1}{2} i_{dqs}^{rT} \frac{dl_{dq}}{d\theta_e} i_{dqs}^r + i_{dqs}^{rT} \frac{d\lambda_{dqs}^r}{d\theta_e} + (L_d - L_q) i_{dq}^r i_{qs}^r + \Lambda_{PM} i_{qs}^r\right) + T_{cog} \quad (12)$$

where L_d, L_q and Λ_{PM} are the average value of the dq-axes inductances and d-axis flux, respectively.

It can be observed from (12) that knowledge of the spatial distribution of both flux and inductances is required for the precise modelling of PMSM torque. It has to be noted that both inductances and flux will change with the fundamental current due to magnetic saturation [33]-[34]. Precise implementation of (12) is not viable, the use of accurate, high bandwidth torque sensors being therefore needed for precise machine characterization.

B. FEA analysis of torque pulsations

This subsection analyzes, using finite element analysis, the torque harmonic components in PMSMs and which will be further correlated with the experimental results. It is noted that mismatches between the model and the real machine should be expected due to assembling tolerances and/or mismatches between real materials and modelled materials.

Fig. 1 shows the schematic representation of the machine that will be used both for simulation and experimental verification, the parameters being shown in Table I. The machine is a 36s/6p IPMSM. Fig. 2a shows the output torque obtained by FEA when the test machine is operated with negative d-axis current i.e. flux-weakening current (-14A) and constant rotational speed of 20rad/s, while Fig. 2b shows the corresponding FFT. FEA has been performed with nonlinear B-H curves for the rotor and stator core and PMs materials, therefore saturation induced effects can be computed. Perfectly sinusoidal current will be used, torque being calculated using the nodal force method.

As predicted by (5)-(7), the 18th and 36th are the most relevant torque harmonic order components. The LCM between the number of stator slots and rotor poles is 36; consequently, T_{cog} will have a frequency equal to $36\omega_r$ (5). Additionally, when fundamental current is applied, torque ripple will appear at integer multiples of 6 times the electrical frequency (7), i.e. $18\omega_r$, $36\omega_r$, ...

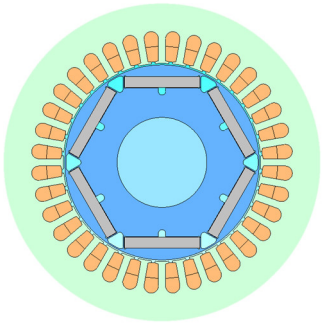

Fig. 1.- 36s/6p IPMSM design.

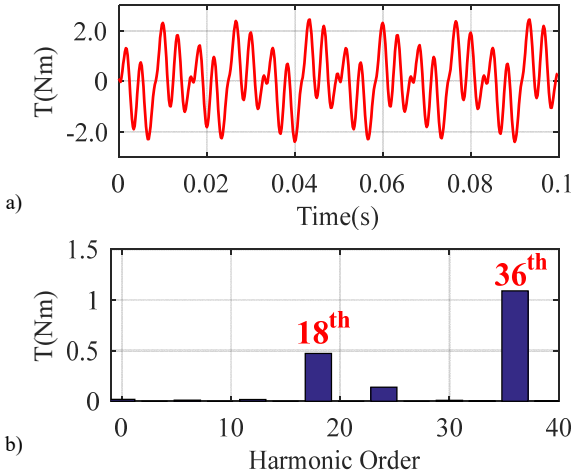

Fig. 2.- Simulation results. a) Electromagnetic torque of 36s/6p IPMSM and b) FFT. I_d= -1pu, I_q= 0pu, ω_r= 20rad/s.

TABLE I. IPMSM PARAMETERS

P_{RATED}	T_{RATED}	V_{RATED}	I_{RATED}	ω_r	Poles	Slots
4 kW	39 Nm	350 V	14 A	1800 rpm	6	36

III. Torque ripple measurement using strain gauges-based torque sensors analysis

The most common option for measuring torque ripple are strain gauges based systems [19], [25]. However, measuring torque directly from the rotor shaft by using traditional torque measurement sensors based on the shaft torsion measurement (e.g. rotary torque transducers, see Fig. 3) will not be a valid indication of the motor torque if mechanical resonant frequencies affect the frequency measurement range. If the torque pulsations components to be measured are closed the torsional resonant frequency of the test bench, their magnitude could be amplified before they are measured [25]. Bandwidth of the torque sensor measurement systems is often considered to be a limiting factor; however, the resonant frequency of the test bench, which is usually ignored, can seriously compromise the measurements.

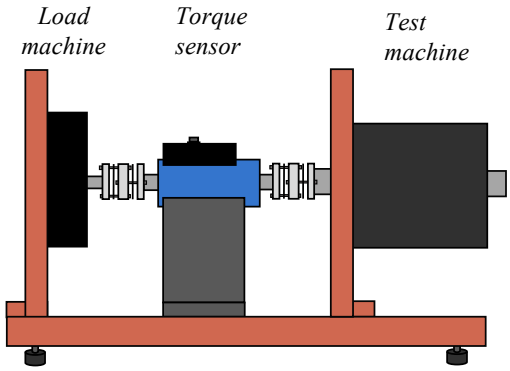

Fig. 3.- Test bench design for measuring torque ripple using a torque sensor.

In a test bench including the test machine and a load machine, the rotor shaft can be modeled as a spring-damper system, the whole system can be considered to be a single degree of freedom (SDOF) two mass-spring-damper system. Under this assumption, the system resonant frequency is defined by (13) [19], [25], [32].

$$f_{res} = \frac{1}{2\pi}\sqrt{\frac{K_{tot}}{J_{eff}}} \tag{13}$$

where K_{tot} is the torsional stiffness of the test bench and J_{eff} is the total inertia of the system. The effective inertia of a two mass-spring damper system, J_{eff}, can be calculated as (14) [32].

$$J_{eff} = \frac{1}{\frac{1}{J_{PMSM}} + \frac{1}{J_{LM}}} \tag{14}$$

where J_{PMSM} is the inertia of the test machine and J_{LM} is the inertia of the load machine. Both values include the inertia of the flexible couplings needed for connecting the torque sensor.

Traditional torque transducers add two flexible elements in series with the rotor shaft as shows Fig. 3; the torque sensor and an additional mechanical coupling between the torque sensor and the test machine. The total torsional stiffness of the system, K_{tot}, is therefore given by (15).

$$\frac{1}{K_{tot}} = \frac{1}{K_{sens}} + \frac{1}{K_{shaft}} + \frac{1}{K_{coupling1}} + \frac{1}{K_{coupling2}} \tag{15}$$

where K_{shaft} is the torsional stiffness of the shaft defined by (16), $K_{coupling1}$ and $K_{coupling2}$ are the torsional stiffness of the mechanical couplings and K_{sens} is the torsional stiffness of the torque sensor [32]. It has to be noted that the torsional stiffness of the mechanical couplings is around two full orders of magnitude bigger than the sensor torsional stiffness and 8.5 times bigger than the shaft torsional stiffness (see Table III). The overall stiffness of the system (15) can be modeled as two flexible elements (sensor and shaft) in series.

$$K_{shaft} = \frac{G_{steel}\pi d_{shaft}^{4}}{32L_{shaft}} \tag{16}$$

where G_{steel} is the modulus of rigidity of the shaft material, d_{shaft} is the shaft diameter and L_{shaft} is the length of the shaft.

It can be concluded from (13)-(16) that to increase the torsional resonant frequency, and therefore to increase the measurement frequency range, the effective inertia should be decreased or the total stiffness should be increased. Inertia of the system is fixed by the motor to be tested and the load motor, consequently variation of the system stiffness, see (13), is the only viable option to change the system resonant frequency.

It can be concluded from (15)-(16) that the total system stiffness can be increased by: 1) using a stiffer sensor; 2) reducing the effective shaft length. In [25], it has been shown that a sensor of 8 times more stiffness, will increase the system bandwidth by 2.8 times if the stiffness of the shaft and joints are sufficiently larger to be neglected. However, the working principle of torque transducers based on the measurement of the torsional force produced by the displacement of an element of known stiffness (i.e. strain gauges' torque sensors), limits the stiffness of the sensor [25]. In addition, placing a torque transducer in the test bench for measuring torque ripple also increases the total length of the shaft, see Fig. 3, reducing therefore the shaft stiffness (16).

Another limiting factor for measuring torque pulsation from traditional torque measurement systems is resolution due to the fact that torque transducer must be scaled for the nominal (average) torque of the machine, meaning that only a portion of the overall range will be excited by the torque ripple.

IV. Shaft-mounted accelerometer-based torque pulsations measurement

As seen in (1), torque pulsations can be measured by measuring the shaft angular acceleration. The linear acceleration at a point of the rotor shaft, $\vec{a}$ (17), can be split into centrifugal a_c (x-axis) (18) and tangential a_t (y-axis) acceleration (19) components (see Fig. 4). Centrifugal acceleration is given by (18), r being the distance from the point to the center of the shaft, g the Earth's gravity, a_{ch} the magnitude of the hth harmonic component of the centrifugal acceleration, h the harmonic order of the hth harmonic component and φ_{ch} the

phase of the h[th] harmonic component of the centrifugal acceleration. A general expression of the tangential acceleration, a_t, is given by (19), where a_{th} is the magnitude of the h[th] harmonic component of the tangential acceleration, φ_{th} is the phase of the h[th] harmonic component of the tangential acceleration. After decoupling gravity form the tangential acceleration measurements (19), (20) is obtained, $a_t^{'}$; i.e. $a_t^{'}$ contains only accelerations resulting from torque pulsations. It can be observed from (21) that $a_t^{'}$ is proportional to the distance of the point to the center of the shaft, r, and to the angular acceleration α_r (1), being also independent of the rotor speed.

$$\bar{a} = a_c + ja_t \tag{17}$$

$$a_c = r\omega_r^{\,2} + g\cos(\omega_r t) + \sum_{h=1}^{\inf} a_{ch}\cos(h\omega_r t + \varphi_{ch}) \tag{18}$$

$$a_t = g\sin(\omega_r t) + \sum_{h=1}^{\inf} a_{th}\sin(h\omega_r t + \varphi_{th}) \tag{19}$$

$$a_t^{'} = a_t - g\sin(\omega_r t) = \sum_{h=1}^{\inf} a_{th}\sin(h\omega_r t + \varphi_{th}) \tag{20}$$

$$a_t^{'} = r\alpha_r \tag{21}$$

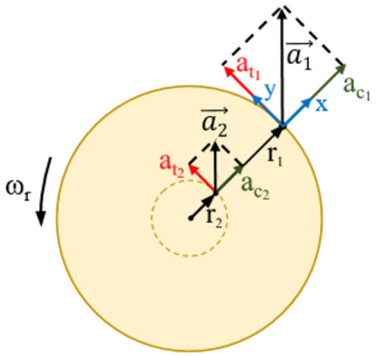

Fig. 4.- Decomposition of the acceleration vector of a rotating body.

The system proposed in this paper measures the linear tangential acceleration a_t by attaching a linear accelerometer directly to the rotor shaft as shown Fig. 5.

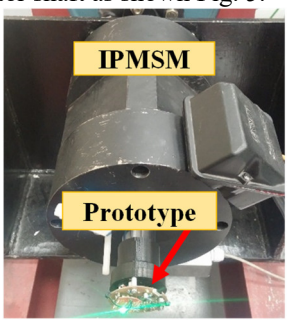

Fig. 5.- IPMSM with the wireless acceleration measurement system.

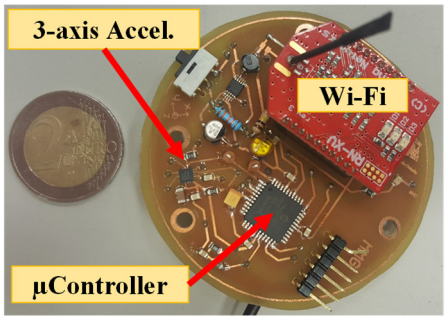

Fig. 6.- Experimental setup used for rotor acceleration measurement

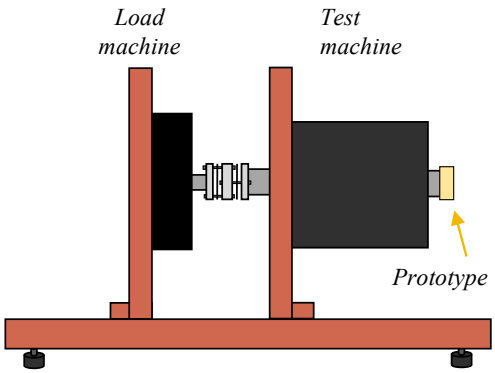

Fig. 7.- Test bench design for measuring torque ripple using the proposed shaft-mounted torque pulsations measurement system.

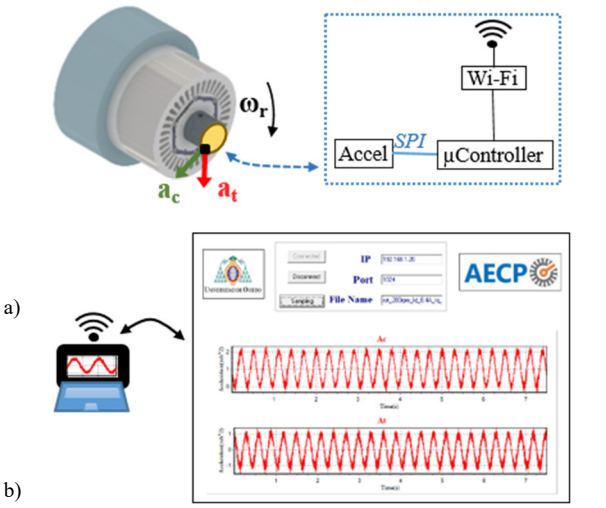

Fig. 8.- (a) Schematic representation of the torque pulsation measurement system and (b) desktop application.

The prototype is shown in Fig. 6, its main characteristics are shown in Table II. A schematic representation of the measurement system is shown in Fig. 8a; it includes a three-axis digital MEMS capacitive accelerometer [36], µController, battery and Wi-Fi module. Accelerometer signals are acquired by a µController and transmitted using a Wi-Fi link to a central computer (see Fig. 8a). Data transmission has been performed using a TCP/IP communication protocol in order to ensure reliable transmission of packets. The accelerometer has a selectable sample rate ranging from 12.5 Hz to 25.6 kHz with

an integrated anti-aliasing filter which cut-off frequency is half of the sampling frequency (i.e. the bandwidth of the system being therefore half of the sampling frequency). A sampling rate of 1 kHz was used for the experiments shown in this paper as a trade-off between resolution and noise immunity. To supply the three-axis digital accelerometer, µController and wireless transmission device, a power stage composed of a Li-Po battery and DC-DC converters, was included; To minimize the additional oscillations caused by the connection of an additional weight to the rotor shaft (see Fig. 7), the components of the prototype have been uniformly distributed across the PCB. System balance has been verified by means of a dedicated equilibration test, balance quality (Q) of 2.5 according to ISO-1940-1 has been measured. The PCB has been directly attached to the rotor shaft using a PLA support.

Fig. 8b shows a screenshot of the desktop application that has been developed.

Fig. 9a shows an example of the tangential acceleration, a_t, measurement; Fig. 9b shows the corresponding FFT. It is observed from Fig. 9b that there is a component in the tangential acceleration at ω_r due to gravity, the rest of harmonics (i.e. $6\omega_r$, $18\omega_r$, $36\omega_r$,..) being produced by torque pulsations of the test machine.

Compared to strain gauges based sensors, the proposed system reduces the flexible elements (see Fig. 7), resulting therefore in a stiffness increase; the total stiffness of the system can be rewritten as (22) when using the proposed system.

$$\frac{1}{K_{tot}} = \frac{1}{K_{shaft}} + \frac{1}{K_{coupling1}} \tag{22}$$

Additionally, the total effective shaft length will be also reduced, which also results in a stiffness increase (see (16)).

TABLE II. MAIN CHARACTERISTICS OF THE MEASUREMENT SYSTEM

Resolution/Sensitivity	16-bits
Measurement range	-78.4 m/s^2 to 78.4 m/s^2
Bandwidth	12.8 kHz
Number of sensors	1 (3-axis)
Output Noise	1.3 mm/s^2/$\sqrt{Hz}$

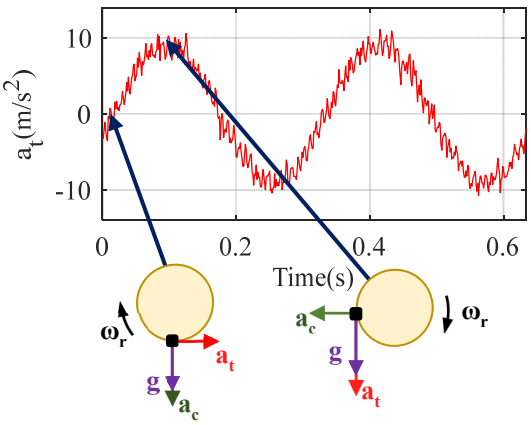

a)

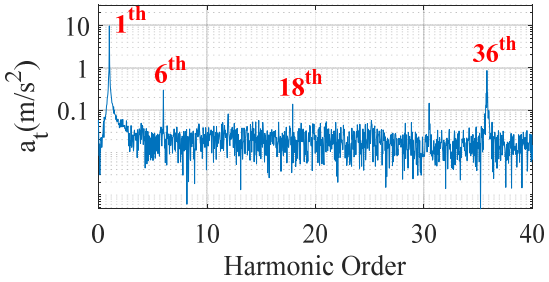

b)

Fig. 9.- Experimental results: a) Tangential acceleration (a_t) measurement and b) FFT of a_t. I_d= -1pu, I_q= 0pu, ω_r= 20rad/s.

On the other hand, the effective inertia of the system when attached the proposed designed to the rotor shaft of the test machine can be defined by (23).

$$J_{eff} = \frac{1}{\frac{1}{J_{PMSM+MS}} + \frac{1}{J_{LM}}} \tag{23}$$

where $J_{PMSM+MS}$ is the inertia of the test machine adding the inertia of proposed pulsation measurement system. Since the weight of the designed prototype (110g) is 60 times lighter than the test motor (6.6 Kg), the additional inertia can be neglected.

It is finally noted that, in addition to the increased system bandwidth, the designed torque pulsation measurement system measures the torque pulsations independently of the average torque (20).

V. Experimental results

Experimental results have been conducted using the IPMSM shown in Fig. 1 and Fig. 5. The test bench can be seen in Fig. 10; its main characteristics are summarized in Table III. To assess the accuracy of the torque pulsations measurement system, output torque of the test machine has been measured with an Interface Torque transducer [20] (T5 model, 12-Bit resolution, 10kHz, ±100Nm). The torsional resonance frequency of the test bench when including the torque transducer is 170Hz while it increases to 595Hz when replacing the torque transducer by the proposed system (i.e. 3.5 times increase of the resonant frequency).

As it was stated in the previous section, torque ripple and cogging torque of the test machine will overlap at 36th harmonic component. A strain gauges torque transducer will be used to assess the performance of the proposed measurement system. To avoid the aforementioned resonance issues, the maximum motor speed is limited to 4.77 Hz (i.e. 172Hz/36; torsional resonance frequency of the test bench when including the torque transducer over torque ripple and cogging torque harmonic component). Experimental results have been conducted at 3.18Hz to ensure that the measured harmonics will not be disturbed by the mechanical resonances of the test bench.

The speed of the test bench has been fixed with a commercial 40kW axial PMSM machine (EMRAX 228 [37]). Table IV shows the load machine parameters. The speed control loop has a bandwidth of 8Hz; 18th and 36th harmonic components at a rotational speed of 3.18Hz are therefore

beyond the speed control loop bandwidth. The LCM between the number of stator slots and rotor poles is 90; consequently, T_{cog} of the load machine will be a 90^{th} harmonic component. Since the cogging torque harmonic order of the load machine is more than doubled compared with the test machine, torque pulsations components of the test machine can be easily distinguished.

The test IPMSM is equipped with the rotor acceleration measurement system shown in Fig. 6. Fig. 11a shows the measured torque using the torque transducer shown in Fig. 10, Fig. 11b shows the tangential acceleration, while Fig. 11c shows the signal after decoupling gravity. This can be done by means of a band-stop filter (BSF) at the rotating frequency of the machine (see. Fig. 9a). A discrete second-order Butterworth BSF with a bandwidth of 2Hz has been used in Fig. 11c.

Isolation of specific high frequency components from the measured torque (see Fig. 11a) or from the tangential rotor acceleration measurements (see Fig. 11c), has been performed by means of band-pass filters (BPF) at the corresponding harmonic component frequency $h\omega_r$, where h stands for the harmonic order; second-order Butterworth BPF with a bandwidth of 2Hz has been used.

Fig. 12a and Fig. 12b shows the magnitude of the 18^{th} and 36^{th} of the measured tangential rotor acceleration and of the measured output torque (using the torque transducer) vs. I_q when I_d=0. Since output torque and tangential rotor acceleration are proportional (see (1)), both measurements have been directly compared to minimize the manipulation of the measured data. Fig. 13a and Fig. 13b show analogous results to Fig. 12 but when I_d is changing and I_q=0. All experimental results shown in this section have been obtained in steady state conditions. It is observed from Fig. 12 that torque ripple is independent of the sign of q-axis current, which was an expected result due to the symmetric behavior of the machine with respect to the d-axis. On the other hand, torque ripple will depend on the sign of d-axis current (see Fig. 13). When the machine operates in the flux-weakening region (I_d<0), flux due to negative d-axis current partially counteracts the PM flux (assuming d-axis being aligned with the PMs), and, on the contrary, flux due to positive d-axis current adds to the PM flux (flux-intensifying current). Consequently, asymmetric harmonic trend depending on the d-axis current sign is expected.

It can be also noted from Fig. 12a and Fig. 13a that variation of 18^{th} harmonic component of the torque (i.e. torque ripple) with I_q and I_d is seen to be almost linear, torque ripple being zero when no current is being injected. On the contrary, the cogging torque (36^{th} torque harmonic component when I_d=I_q=0), see Fig. 12b and Fig. 13b, is not zero when no current is being injected, its magnitude being significantly larger than the 18^{th} harmonic component; i.e. the most relevant source of torque pulsation in this machine is the cogging torque.

Precise measurement of the accuracy of the proposed method at high speeds is not trivial, as in this case the test bench will be affected by the resonances due to the strain gauges sensor, this task being a matter of ongoing research.

It can be concluded from the experimental results shown in Fig. 12 and Fig. 13 that the tangential acceleration measured using the proposed torque pulsation measurement system matches the torque harmonics measured by the torque transducer, demonstrating therefore the viability of the proposed torque pulsation measurement system.

TABLE III. MAIN CHARACTERISTICS OF THE TEST BENCH SYSTEM

J_{IPMSM}	Inertia of the test machine	92.1 kgcm^2
J_{LM}	Inertia of the load machine	383.1 kgcm^2
K_{sens}	Torque sensor stiffness	$9.7 \cdot 10^3$ Nm/rad
$K_{coupling}$	Mechanical coupling stiffness	$7.25 \cdot 10^5$ Nm/rad
G_{steel}	Modulus of rigidity for the shaft material	$80 \cdot 10^9$ Pa
d_{shaft}	Shaft diameter	5.56 cm
L_{shaft}	Shaft length	88 cm

TABLE IV LOAD MACHINE PARAMETERS

P_{RATED}	T_{RATED}	I_{RATED}	ω_r	Poles	Slots	LCM(Q,P)
40 kW	125 Nm	160 A	3000 rpm	20	18	90

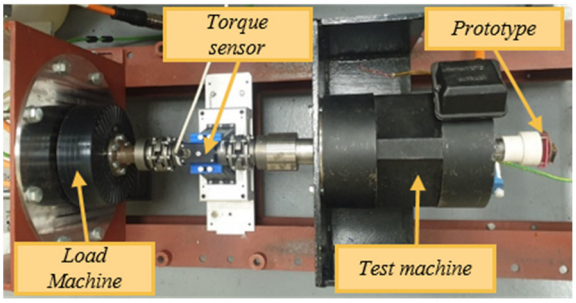

Fig. 10.- Picture of the test bench.

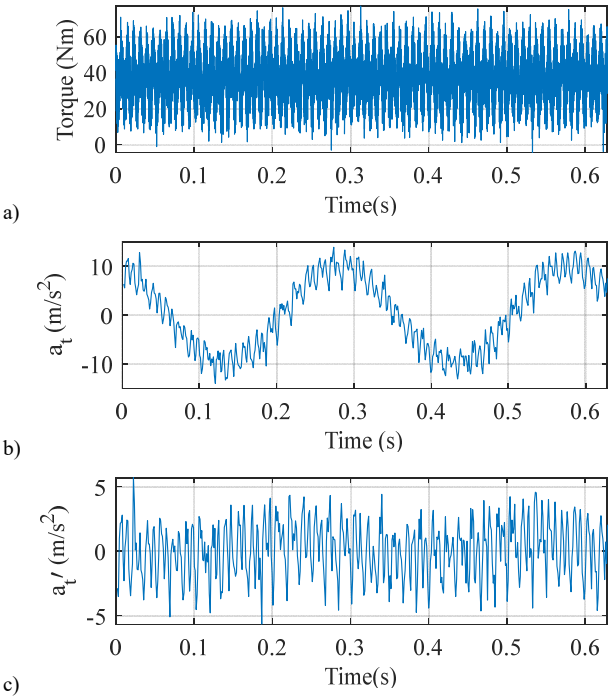

Fig. 11.- Experimental results: a) Output torque measurement, b) Tangential acceleration (a_t) (19) c) Tangential acceleration (a_t') after decoupling the gravity acceleration component (20). I_d= 0pu, I_q= 1pu, ω_r= 20rad/s

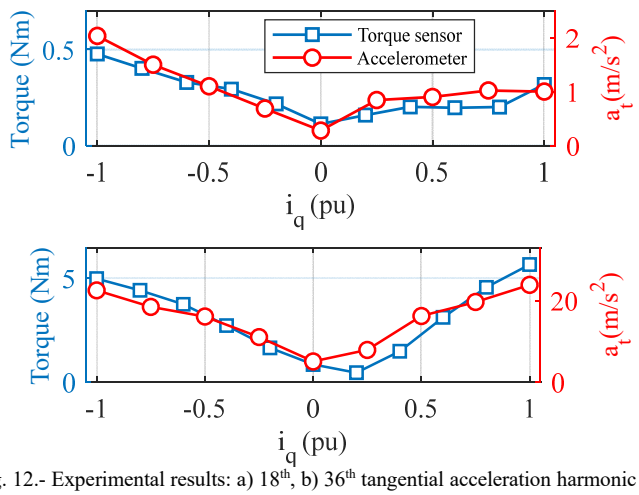

Fig. 12.- Experimental results: a) 18th, b) 36th tangential acceleration harmonic components and torque harmonic components measurements vs I_q current. ω_r= 20rad/s.

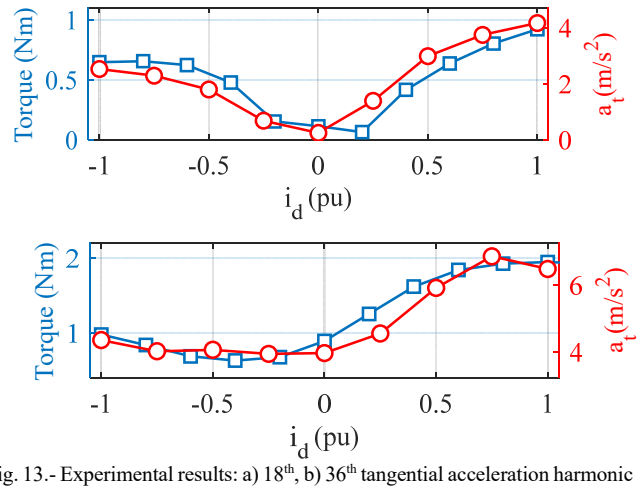

Fig. 13.- Experimental results: a) 18th, b) 36th tangential acceleration harmonic components and torque harmonic components measurements vs I_d current. ω_r= 20rad/s.

VI. Conclusions

A shaft-mounted torque ripple measurement system has been presented in this paper. Analytical models and FEA have been used to determine the main characteristics of the torque pulsations, from which the requirements for the measurement system have been stablished. The system uses a shaft-mounted 3D digital MEMS capacitive accelerometer, and can operate at any load level, provides high accuracy, independently of the torque ripple to average torque ratio, and increasing the stiffness of the test system since no mechanical couplings are needed. Experimental results have been provided to confirm the performance of the measurement system.

VII. References

[1] D. W. Novotny and T.A. Lipo, "Vector Control and Dynamics of AC Drives" Oxford Science Publications, 1996.

[2] Duane C. Hanselman, "Brushless Permanent Magnet Motor Design" New York: Mc-Graw Hill, 1994.

[3] D. Reigosa, D. Fernandez, Y. Park, A. B. Diez, S. B. Lee and F. Briz, "Detection of demagnetization in permanent magnet synchronous machines using hall-effect sensors," IEEE Energy Conversion Congress and Exposition (ECCE), pp. 4686-4693, Oct. 2017

[4] D. Reigosa, D. Fernandez, C. Gonzalez, S. B. Lee and F. Briz, "Permanent magnet synchronous machine drive control using analog hall-effect sensors," IEEE Energy Conversion Congress and Exposition (ECCE), pp. 3966-3971, Oct. 2017.

[5] B. Saunders, G. Heins, F. De Boer and M. Thiele, "Cogging torque estimation for sensorless PMSM," International Conference on Electrical Machines (ICEM), 2949-2954, Sept. 2012.

[6] M. Piccoli, and M. Yim. "Cogging Torque Ripple Minimization via Position Based Characterization." Robotics: Science and Systems, 2014.

[7] O. Pyrhonen and P. Eskelinen, "Advanced measurement of rotor vibration in electric drives." IEEE Aerospace and Electronic Systems Magazine, vol.13, no. 5, pp. 21-23, May 1998.

[8] J. C. Urresty, R. Atashkhooei, J. R. Riba, L. Romeral and S. Royo, "Shaft Trajectory Analysis in a Partially Demagnetized Permanent-Magnet Synchronous Motor." IEEE Transactions on Industrial Electronics, vol. 60, no. 8, pp. 3454-3461, Aug. 2013.

[9] Z. Azar, Z. Q. Zhu and G. Ombach, "Influence of Electric Loading and Magnetic Saturation on Cogging Torque, Back-EMF and Torque Ripple of PM Machines." IEEE Transactions on Magnetics, vol. 48, no. 10, pp. 2650-2658, Oct. 2012.

[10] X. Ge and Z. Q. Zhu, "Sensitivity of Manufacturing Tolerances on Cogging Torque in Interior Permanent Magnet Machines With Different Slot/Pole Number Combinations." IEEE Transactions on Industry Applications, vol. 53, no. 4, pp. 3557-3567, July-Aug. 2017.

[11] S. Rojas, M. A. Pérez, J. Rodríguez and H. Zelaya, "Torque ripple modeling of a permanent magnet synchronous motor." IEEE International Conference on Industrial Technology (ICIT), pp. 433-438, March 2010.

[12] D. H. Lee, C. L. Jeong and J. Hur, "Analysis of cogging torque and torque ripple according to unevenly magnetized permanent magnets pattern in PMSM." IEEE Energy Conversion Congress and Exposition (ECCE), pp. 2433-2438, Oct. 2017.

[13] H. Jussila, P. Salminen, M. Niemela, and J. Pyrhonen, "Guidelines for Designing Concentrated Winding Fractional Slot Permanent Magnet Machines." International Conference on Power Engineering, Energy and Electrical Drives (POWERENG), pp. 191-194, April 2007.

[14] L. Dosiek and P. Pillay, "Cogging Torque Reduction in Permanent Magnet Machines." IEEE Transactions on Industry Applications, vol. 43, no. 6, pp. 1565-1571, Nov.-Dec. 2007.

[15] N. Bianchi and S. Bolognani, "Design techniques for reducing the cogging torque in surface-mounted PM motors" IEEE Transactions on Industry Applications, vol. 38, no. 5, pp. 1259-1265, Sep./Oct. 2002.

[16] C. Studer, A. Keyhani, T. Sebastian and S. K. Murthy, "Study of cogging torque in permanent magnet machines." IEEE Industry Applications Society Annual Meeting (IAS), pp. 42-49 vol.1, Oct. 1997.

[17] H. Le-Huy, R. Perret and R. Feuillet, "Minimization of Torque Ripple in Brushless DC Motor Drives." IEEE Transactions on Industry Applications, vol. 22, no. 4, pp. 748-755, July 1986.

[18] Z. Q. Zhu and D. Howe, "Influence of design parameters on cogging torque in permanent magnet machines." IEEE Transactions on Energy Conversion, vol. 15, no. 4, pp. 407-412, Dec 2000.

[19] A. Schramm, E. Sworowski and J. Roth-Stielow, "Methods for measuring torque ripples in electrical machines." IEEE International Electric Machines and Drives Conference (IEMDC), pp. 1-8, May 2017.

[20] Interface force measurement solutions. Torque transducers: T5, 2019. Available at https://www.interfaceforce.com/products/torque-transducers/t5-standard-precision-pedestal-mount-shaft-style-rotary-torque-transducer/, accessed 16-October-2019.

[21] HBM. HBM torque sensors. Available at https://www.hbm.com/en/0264/torque-transducers-torque-sensors-torque-meters/, accessed 16-October-2019.

[22] Futek. Futek torque sensors. Available at https://www.futek.com/store/Torque%20Sensors, accessed 16-October-2019.

[23] Magtrol motors testing & sensors. Magtrol torque transducers. Available at https://www.magtrol.com/product-category/torque-transducers/, accessed 16-October-2019.

[24] Zhu, Z. Q. “A simple method for measuring cogging torque in permanent magnet machines.” IEEE Power & Energy Society General Meeting (PES), pp. 1-4, July 2009.

[25] G. Heins, M. Thiele and T. Brown, “Accurate Torque Ripple Measurement for PMSM.” IEEE Transactions on Instrumentation and Measurement, vol.60, no. 12, pp. 3868-3874, Dec. 2011.

[26] L. Ferraris, F. Franchini and E. Poskovic, “The cogging torque measurement through a new validated methodology.” IEEE International Conference on Compatibility, Power Electronics and Power Engineering (CPE-POWERENG), pp. 398-403, April 2017

[27] Binsfeld. Temporary torque measurement: Torquetrak 10K. Available at https://binsfeld.com/torquetrak/temporary-torque-measurement/torquetrak-10k/, accessed 15-March-2020

[28] KMT. KMT Telemetry sensors: 1-channel telemetry for rotating shafts. Available at https://www.kmt-telemetry.com/telemetry/1-channel-telemetry/tel1-pcm-flex-ind/, accessed 15-March-2020

[29] L. Baghli, J. F. Pautex and S. Mezani, "Wireless instantaneous torque measurement, application to induction motors,"The XIX International Conference on Electrical Machines - ICEM 2010, Rome, 2010, pp. 1-6.

[30] M. Martinez, D. Fernandez, D. Reigosa, J. M. Guerrero and F. Briz, “Wireless Torque Pulsations Measurement System for PMSMs.” IEEE Energy Conversion Congress and Exposition (ECCE), pp. 1668-1673, Sept. 2018.

[31] G. Liu, X. Du, W. Zhao and Q. Chen, "Reduction of Torque Ripple in Inset Permanent Magnet Synchronous Motor by Magnets Shifting." IEEE Transactions on Magnetics, vol. 53, no. 2, pp. 1-13, Feb. 2017.

[32] William T. Thomson, “Theory of vibration with applications”. Fourth edition 1993.

[33] C. Lai, G. Feng, K. Mukherjee, V. Loukanov and N. C. Kar, "Torque Ripple Modeling and Minimization for Interior PMSM Considering Magnetic Saturation," in IEEE Transactions on Power Electronics, vol. 33, no. 3, pp. 2417-2429, March 2018.

[34] N. Nakao and K. Akatsu, "Suppressing Pulsating Torques: Torque Ripple Control for Synchronous Motors," in IEEE Industry Applications Magazine, vol. 20, no. 6, pp. 33-44, Nov.-Dec. 2014.

[35] T. M. Jahns and W. L. Soong, "Pulsating torque minimization techniques for permanent magnet AC motor drives-a review," in IEEE Transactions on Industrial Electronics, vol. 43, no. 2, pp. 321-330, April 1996.

[36] Kionix. Kionix accelerometers KX124-1051, 2019. Available at https://www.kionix.com/product/KX124-1051, accessed 16-October-2019.

[37] Emrax e-motors. Standard motors: Emrax 228, 2019. Available at https://emrax.com/products/emrax-228, accessed 16-October-2019.